Subcellular Distribution of Dietary Methyl-Mercury in Gammarus fossarum and Its Impact on the Amphipod Proteome

Claudia Cosio, Davide Degli-Esposti, Christine Almunia, Véronique Gaillet, Hervé Sartelet, Jean Armengaud, Arnaud Chaumot, Olivier Geffard, Alain Geffard

Subcellular distribution of dietary methyl-mercury in *Gammarus fossarum* and its impact on the amphipod proteome

Claudia Cosio[a]*, Davide Degli-Esposti[b], Christine Almunia[c], Véronique Gaillet[a], Hervé Sartelet[d], Jean Armengaud[c], Arnaud Chaumot[b], Olivier Geffard[b], Alain Geffard[a]

[a] Université de Reims Champagne-Ardenne, UMR-I 02 INERIS-URCA-ULH SEBIO, Campus du Moulin de la Housse, CEDEX, Reims, BP 1039 51687, France

[b] INRAE,UR RiverLy, Laboratoire d'écotoxicologie, F-69625 Villeurbanne , France.

[c] Université Paris-Saclay, CEA, INRAE, Département Médicaments et Technologies pour la Santé (DMTS), SPI, 30200 Bagnols-sur-Cèze, France

[d] Université de Reims Champagne-Ardenne, UMR CNRS/URCA 7369, Matrice Extracellulaire et Dynamique Cellulaire (MEDyC), Campus du Moulin de la Housse, CEDEX, Reims, BP 1039 51687, France

*Corresponding author: Claudia.Cosio@univ-reims.fr,

Abstract

The transfer of methyl-Hg (MeHg) from food is central for its effects in aquatic animals, but we still lack knowledge concerning its impact in invertebrate primary consumers. In aquatic environments, cell walls of plants are particularly recalcitrant to degradation and as such remain available as food source for long periods. Here, the impact at the proteomic level of dietary MeHg in *Gammarus fossarum* was established and linked to subcellular distribution of Hg.

Individuals of *G. fossarum* were fed with MeHg in cell wall or intracellular compartments of *Elodea nuttallii*. Hg concentrations in subcellular fractions were 2 to 6x higher in animals fed with cell wall than intracellular compartments. At the higher concentrations tested, the proportion of Hg in metal sensitive fraction increased from 30.0±6.1% to 41.0±5.7% for individuals fed with intracellular compartment, while biologically detoxified metals fraction increased from 30.0±6.1% to 50.0±2.8% when fed with cell wall compartment. Data suggested that several thresholds of proteomic response are triggered by increased bioaccumulation in each subcellular fraction in correlation with Hg exclusively bound to the metal sensitive fraction, while the increase of biologically detoxified metal likely had a cost for fitness. Proteomics analysis supported that the different binding sites and speciation in shoots subsequently resulted in different fate and cellular toxicity pathways to consumers.

Our data confirmed that Hg bound in cell walls of plants can be assimilated by *G. fossarum*, which is consistent with its feeding strategy, hence pointing cell walls as a significant source for Hg transfers and toxicity in primary consumers. The high accumulation of Hg in macrophytes make them a risk for food web transfer in shallow ecosystems. The present results allowed gaining new insights on the effects and uptake mechanisms of MeHg in aquatic primary consumers.

Keywords: bioaccumulation; cell walls; cytosol; proteogenomics; subcellular distribution.

Synopsis: subcellular compartmentalization of MeHg in shoots determines its fate and toxicity in primary consumers

52

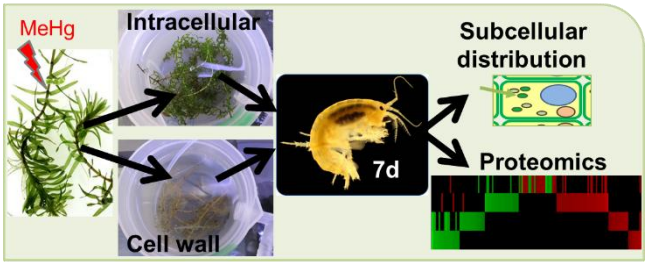
MeHg
Intracellular
Cell wall
7d
Subcellular distribution
Proteomics

53

54

Introduction

Mercury (Hg) is a global pollutant seriously threatening ecosystems and eventually health, due to the biomagnification of methyl-Hg (MeHg) through the food chain [1, 2, 3]. Past Hg deposits of anthropogenic sources continue to cycle through compartments, forming up to 60% of current Hg emissions [4]. Consequently, even if new emissions of Hg are kept constant, Hg deposition will increase in the future [5, 6, 7]. In this context, understanding how Hg is bioaccumulated and biomagnified in food webs is central to increase the effectiveness of environmental management programs for biota and human health. For example, aquatic plants are key species in shallow aquatic environment in which MeHg is formed [8]. The high accumulation of Hg in aquatic plants make them considered a model species for phytoremediation programs, biomonitoring or to perform ecotoxicological tests [9], but also at risk for food web transfer [10, 11]. A current research priority is to establish the sources of dietary Hg having a detrimental impact in aquatic plant-based food webs for mitigation programs.

Both inorganic Hg (IHg) and MeHg are bioaccumulated in biota. While MeHg generally represents 0.05 to 1% and up to 30% of total Hg (THg = IHg + MeHg) in water, MeHg forms up to 80-100% of the THg in fish muscles, resulting in very high toxic body burdens in fish, therefore threatening humans' health through fish consumption [2, 12, 13]. Consequently, although both IHg and MeHg trigger toxicity in biota, in animals dietary MeHg is the main risk of Hg [2, 12]. Nonetheless, a major gap in knowledge concerns the impact of dietary Hg uptake in invertebrate primary consumers. Data supported the oxidative stress to be central for MeHg toxicity in aquatic animals [14, 15], but few studies concern effects through diet at environmental concentrations and none concern invertebrates [16]. In this context, the impact of MeHg in realistic environmental exposure scenarios and representative biota need to be studied to better anticipate its potential environmental impact. In aquatic invertebrates, toxicity and tolerance of metal accumulation can be explained by its subcellular partitioning [17]. For example, in biota the sequestration of toxic metal by metallothioneins and granules is known as biologically detoxified metals (BDM), while the partition in the metal sensitive fraction (MSF) is expected to cause the toxicity [17, 18]. Moreover, linking intracellular concentration and distribution to molecular and cellular responses is a current research priority in biomonitoring, as it could participate in revealing innovative biomarkers for environmental risk assessment [9, 19].

Pioneer studies on diatoms suggested that intracellular MeHg was primarily transferred to copepods, while Hg from cell walls, consisting in silicate frustules, was not assimilated [20]. By contrast, we recently demonstrated that IHg and MeHg from cell walls -formed primarily of

cellulose, hemicellulose and pectin- in shoots of the macrophyte *Elodea nuttallii* resulted in a higher transfer to gammarids than intracellular Hg [10]. Similarly, chironomids fed with shopped macrophytes, to mimic incorporation in sediments of decaying tissues, revealed that MeHg was more transferable to sensitive subcellular targets and bioavailable fraction in primary consumers than IHg found in intracellular or cell wall compartments [11]. Data point that the composition of cell walls could affect the transfer rate of Hg to consumers [10, 11, 21]. The proportion of diatoms in phytoplankton is particularly high in nutrient-rich marine coastal and high latitudes ecosystems, but significantly less in freshwater rivers, lakes and other environments [22, 23, 24]. In this context, data concerning Hg food transfer in marine plankton might not be generalized to other animals with distinct feeding strategies or other ecosystems, including freshwater, brackish water or contaminated sites. Moreover, studies on effect of trophic Hg exposure in primary consumers, i.e. invertebrates are rare [10, 11, 21]. At environmental concentrations, cell walls appeared as the main bioaccumulation compartment of Hg in macrophytes and because of their low degradability are expected to remain for long periods in the aquatic systems, likely serving as food source [25, 26, 27]. Here, we hypothesized that the biding of Hg to plant's cell walls results in a higher dietary transfer and subsequently in a higher toxicity in primary consumers than Hg bound in plant's intracellular compartment. Gammarids as generalist herbivores are instrumental in European lotic ecosystems food webs because of their role in the breakdown of the leaf litter. They are also good bioaccumulators of metals and good candidates for ecotoxicological testing of freshwater ecosystems [19, 28]. *Gammarus* spp are found in *E. nuttallii* beds and were previously reported to feed on the latter [29, 30]. Here we aimed to address how the MeHg localization in *E. nuttallii* shoots (cell wall vs intracellular) defines its subcellular distribution in *G. fossarum*; and how dietary MeHg impacts the proteome of *G. fossarum*. Gammarids were fed for 7 days with either cell wall or intracellular compartment of the plant *E. nuttallii* previously exposed to MeHg and we analyzed the fate and effects of MeHg in animals through subcellular distribution and shotgun proteomics. Extensive proteome profiles further revealed the molecular toxicity pathway of dietary MeHg. This fundamental knowledge contributes to a better knowledge of the fate and impact of dietary MeHg in food webs.

Material and Methods

Labware cleaning

Glasswares and plastic consumables for exposures and sampling were washed for once in detergent, twice in 10% HNO_3, once in 10% HCl, rinsed after each washing step with MilliQ

water (Merck Millipore) and kept in a laminar flow hood until dry. Glass material was in addition heated overnight at 200ºC.

Elodea nuttallii *and* Gammarus fossarum *exposure*

Exposure protocols of *E. nuttallii* and *G. fossarum* were described in [10]. Briefly, shoots were collected in Etournels pounds and acclimated 48h in laboratory conditions. Shoots (10 cm) without roots were exposed to MeHg (CH_3HgCl; Alfa Aesar) or not exposed (control). The exposure concentrations in water were chosen based on previous studies to result in concentrations in shoots after 2h-long exposure spanning lowly to highly contaminated environments (Table S1) [2, 31,]. After the exposure, shoots were washed to conserve the shoot morphology and retain Hg either from intracellular or cell wall compartment. Briefly, intracellular Hg was conserved in shoots by rinsing with 10^{-3} M EDTA (AppliChem) and 10^{-3} M cysteine (Sigma-Aldrich) to remove the extracellular loosely bound Hg[8]. Hg bound in the cell wall were obtained by soaking shoots in methanol-chloroform 3d (Sigma), resulting in lipids solubilization and consequently allowing to recover an intact insoluble cell wall matrix with a conserved structure [32]. This latter method affects cell integrity and organic solvents could cause IHg and MeHg redistribution. As such, concentrations might not be strictly representative of initial concentrations in shoots but was performed to allow feeding animals with purified cell walls.

Gammarus fossarum were sampled in the Bourbre River (France) [33, 34], and acclimatized three weeks to laboratory conditions. Nine 1 cm-long males were fed during 7 days with *E. nuttallii* intracellular (I) or the cell wall (CW) compartments pre-exposed to 4 and 20 µg L^{-1} MeHg concentrations, thereafter referred as 'low' and 'high' MeHg treatments in line with their concentrations corresponding to lowly and highly contaminated environments, respectively [2, 10, 11, 31]. To ensure exclusive exposure of gammarids through plant consumption, water renewal and daily removal of dead individuals was done to avoid exposure to Hg through water or cannibalism, respectively. We observed a weak (15%) mortality of gammarids during exposure in all conditions [10]. This rate agrees with the criteria from the Afnor standard (XP T 90-722-3) for feeding rate measurement in the sentinel species *G. fossarum* [35]. It was not correlated with MeHg concentration, or with the plant compartment (intracellular/cell wall) and supported an absence or a sublethal toxicity in these experimental conditions [10]. No depuration was applied here, based on a former study, using the same experimental exposure conditions showed that a 7 day-long depuration didn't varied Hg concentrations [10].

Subcellular fractionation of Hg in Gammarus fossarum

The fractionation procedure of the whole body (Figure 1) adapted from [17, 36] was described elsewhere [37]. Analyses were done in triplicates. Two frozen gammarids per conditions were homogenized in 1 mL of ice-cold buffer (0.02M Tris-HCl pH 7.5; Sigma-Aldrich, purity 99%). The homogenate (H) was centrifuged 30 min at 4°C at 10,000g. The pellet (P1) was hydrolyzed at 100°C 2 min and 1h with 1M NaOH 65°C and centrifuged 10 min at 10°C at 10,000g, resulting in a supernatant including gut content, cellular debris and likely part of mitochondria (S2), while the pellet contained metal-rich granules and exoskeleton (P2). The supernatant (S1) was ultracentrifuged 30 min at 4°C at 100,000 g forming a pellet (P3) including lysosomes and microsomes and a supernatant (S3) with the cytosol. However, no marker enzymes (i.e. [38, 39]) was used to confirm further the nature of each subcellular fraction besides operational fractions according to [17]. All S3 was further filtered with a sterivex filter (millipore) at 0.45 µm, and thereafter named S4.

High-performance liquid chromatography (HPLC) was performed to fractionate S4 with a column using steric exclusion allowing (BIOSEP-SEC-S 2000; 1 - 300 kDa; Figure S1). Eluting fractions of 0.5 mL were collected up 18 mL, acidified at 0.5% with suprapur HCl (Merx) and kept at 4°C until analyzed. Three pools of metal-ligand were separated: (i) high-molecular weight (HMW; 20-255 kDa) eluting 9 to 15 min after injection, (ii) metallothionein-like protein eluting 16 to 24 min after injection (MTLPs-MW; 1.8-20 –kDa) and (iii) low-molecular weight (LMW; <1.8 kDa) eluting 25 to 35 min after injection. Using this protocol, MTLPs-MW are biologically detoxified metal in cytosol, while the heat sensitive protein (HSeP) or proteins in cytosol is the sum of HMW and LMW [36]. We also summed the area of peaks at 280 nm in these three fractions and normalized them by the biomass used in H. We eventually compared the sum of Hg amounts found in the different subcellular fractions with the fraction H, using H= P2 +S2 + P3 + HMW +MMW + LMW as a quality control, and observed a good agreement (n = 18: 93.4 ± 4.9%). We also injected periodically 1 mM EDTA using the same mobile phase to wash the HPLC column and to verify that Hg concentrations in eluting fractions remained at background level. For the biological interpretation, metal sensitive fraction (MSF) was calculated as P3 + HSeP and biologically detoxified metals (BDM) as P2 + MTLPs-MW. As such, MSF + BDM + S2 = H.

Determination of Hg in gammarids

Pellets, i.e. P2 and P3 fractions, were resuspended in 1 mL water and mineralized 12h at 60°C 30% HNO_3 (suprapur, Merck). THg concentration in P2, S2, P3, S4, MTPLs and HSeP were measured with a MERX-T analytical system (Brooks Rand instrumentsA) using THg method [40] showing a limit of detection (DL) of 0.03 ng·THg·L^{-1}, an error of 2% using certified reference materials (CRMs) ORMS-5 (95.0 ± 1.7 % recovery) and TORT-2 (100 ± 0.1% recovery). MeHg was analyzed in P2, S2, P3, S4, MTPLs and HSeP samples with a MERX-M (Brooks Rand instruments) using MeHg method [41, 42] showing a DL of 0.002 ng·MeHg·L^{-1}, an error of 15% using the CRM TORT-2 (102.5 ± 2.4 % recovery).

Data are presented as arithmetic means ± standard deviations (SD). Normality and homoscedasticity were tested. An analysis of variance (ANOVA, $p < 0.05$) with a post-hoc Tukey's HSD test ($p < 0.05$) was used to perform pairwise comparisons of bioaccumulation in the software R version 3.1.3 [43].

Protein extraction and Tandem mass spectrometry

Proteins were extracted (n= 6) from individuals of *G. fossarum* and identified following the same protocol as formerly described [44]. Briefly, each animal was subjected to a bead beating homogenization using a single 3.2 mm steel bead per tube in LDS buffer (20 µl·mg^{-1}; Invitrogen). Cellular debris were eliminated after centrifugation for 3 min at 10,000 *g*. Proteins from the supernatant were denatured for 5 min at 99 °C. An aliquot of 20 µL was then loaded onto a SDS-PAGE gel for a brief (5 min) electrophoresis as recommended [45]. Each proteome sample was processed and proteolyzed with trypsin (Roche) in ProteaseMAX surfactant (0.01% , Promega) as recommended [46]. Peptides were analyzed with a Q-Exactive HF mass spectrometer (Thermo) operated in data-dependent mode with the same parameters as previously described [47]. Peptides were resolved at a flow rate of 0.2 µL·min^{-1} along a 90 min gradient of CH_3CN in presence of 0.1% formic acid.

Peptide identification and proteomic data analysis

MS/MS spectra were interpreted against the GFOSS database, that is available through PRIDE (accession PXD024583 as GFOSS_db01.fasta) with the MASCOT software (Matrix Science) and the same parameters as those previously described [48]. Proteins were validated on the basis of at least two identified peptides, resulting in a false discovery rate (FDR) lower than 1% as estimated with the decoy database search option. Abundance of each peptide was

measured by their Spectral Count (SC), which corresponds to the count of MS/MS spectra attributed to the same peptide. The protein abundance is the sum of the SC of all the peptides assigned to the protein. Protein abundances were compared between organisms fed with control plants or plants pre-exposed to MeHg. Abundance of Methionine and Cysteine residue content in proteins from each sample was calculated by extracting spectral counts of these residues as previously proposed [49], *i.e.* multiplying the spectral counts of each protein by its number of S-containing residues. The weighted relative abundance in S-containing residues was then obtained by dividing the sum of S-spectral counts by the sum of spectral counts of all residues.

Proteomics data have been deposited to the ProteomeXchange Consortium via PRIDE [50] with the dataset identifier PXD024583 and project DOI 10.6019/ PXD024583

Gene Ontology (GO term) functional annotation, classification and analysis

Identified proteins were annotated in April 2018 using Swissprot (https://www.uniprot.org/) and NCBInr (https://www.ncbi.nlm.nih.gov/protein/) as databases explored with Diamond, a free high-throughput sequence aligner [51]. The NCBInr database was used to find the most probable protein homolog of the closest species to *Gammarus fossarum* for each protein with an e-value below 10^{-10}. The Swissprot database was used to find the top 5 closest proteins in terms of sequence identity to define for each identified protein their biological processes and molecular functions as previously described [52], selecting a bit score alignment above 20 and an e-value below 10^{-4}.

Differential proteomics

The quantities of each protein in animals exposed to treated intracellular or cell wall compartments vs non-treated intracellular or cell wall compartments respectively were compared using Patternlab version 4.0 [53]. The L-stringency was set at 0.6. At least four measurements out of the five replicates per condition were taken into account. The selected data were normalized with the total signal. Proteins were distinguished into 4 groups: the first one corresponds to proteins that satisfied both the F-stringency (<0.30) and statistical criterion (FDR < 0.05); the second one was filtered out by their L-stringency because of the low protein abundance; the third one groups proteins that meet only the fold criterion, and the fourth one comprises proteins that did not satisfy both criteria. Proteins from the first group were selected for the Gene Ontology (GO) slim differential analysis. The average percentage

of S-containing residues in proteins significantly modulated, either over-detected or less-detected, for each comparative test was calculated without specific weight.

GO slim differential analysis

GO slim analysis was performed taking the sum of SC of each GO slim related proteins for each sample. Univariate statistical analysis was performed to define, with the Ttest pValue, the reliability between conditions taking into account the six replicates. The ratio R for each GO slim was calculated for comparing treated conditions and non-treated conditions, either for the intracellular or the cell wall compartment, as the sum of SC of all replicates in the treated samples divided by the sum of SC of all replicates in the control samples. The ratio was compared using "prcomp" from the basic stats package of R to perform a Principal Component Analysis (PCA). From the PCA, significant GOSlim contributing for more than 50 % to distinguish each condition (contrib > 0.5) were extracted.

Results and discussion

Accumulation and subcellular distribution of Hg in G. fossarum

THg concentrations in subcellular fractions were 2 to 6x higher in animals fed with cell wall compartments than intracellular compartment of MeHg pre-exposed plants, and these differences were significant ($p<0.05$; Figure 2). For the high and low MeHg treatment respectively, THg in MSF was 2.9x and 2.0x higher, while BDM 5.8x and 2.3x higher for individuals fed with cell wall than intracellular compartments. To gain insights into transfer dynamics of MeHg in *G. fossarum*, we analyzed by differential centrifugation the subcellular distribution of THg and MeHg (see below) in 3 fractions (Figure 2). In controls and low MeHg treatments, 42.5±6.5% of THg was found in S2 and an equal concentration in MSF and BDM fractions (30.0±6.1%). For gammarids fed with the high MeHg intracellular compartment, the MSF increased (41.0±5.7%), while for the high MeHg cell wall treatment the proportion of THg significantly increased in the BDM (50.0±2.8%; $p<0.05$). We analyzed the spectrograms obtained by HPLC (Figure S1). For example, 5 peaks appeared visually increased and 4 decreased in high MeHg vs ctl cell wall compartments (Figure S1). Because individual peaks are poorly defined by HPLC method used here because bias are caused by the overlapping of peaks, we compared the area of peaks measured at 280 nm in HPLC eluting fractions normalized by the biomass of animals: the area of MTLPs-MW was increased significantly ($p>0.05$) by 1.7±0.1 vs controls in both cell wall treatments and low intracellular treatments. Despite visual differences in peaks (Figure S1), no significant

differences were found for the sum of areas in HMW and LMW between treatments and control. Sequestration of toxic metal by MTs and granules is a very common strategy in biota to control intracellular metal speciation and thus toxicity [17, 18]. MeHg in bivalves and several fish preys was hypothesized to be bound in the intracellular fraction to heat-stable-protein [54, 55]. THg partition between the sensitive (HeSP; 40%) and detoxified (MTLPs-MW; 60%) fractions was previously observed in the cytosol of *C. riparius* exposed to IHg spiked sediments [37]. In the same line, during a 7 day-long depuration phase, both IHg and MeHg concentrations in *G. fossarum* feeding on IHg or MeHg pre-exposed *E. nuttallii* did not significantly vary [10], supporting that in gammarids the accumulated MeHg was bound strongly to biological ligands, i.e. MTs and granules [56, 57, 58]. Here, this detoxification strategy could allow gammarids to reduce the toxicity of the MeHg entering their cytosol when the concentration increased.

Ratio of MeHg as THg was 111±17 % in S2 and S4, 54.3±3.7% in P2 and 60.0±3.8% in P3. Consequently, MeHg proportion as THg increased from 68 to 95% similarly in BDM and MSF in control to high MeHg treatments, respectively (n=3; Table S2). In our previous study with similar feeding of gammarids with *E. nuttallii* [10], bioaccumulation measured on whole individuals hindered to determine where the Hg demethylation took place, e.g. in plant tissues before feeding (for instance, because of plant material decay or biotransformation by microbes), or during digestion or metabolization in gammarids . Here, data supported the second hypothesis, in line with observations made in *C. riparius* of an intracellular demethylation in the insoluble fraction [11]. These observations are consistent with a generalized demethylation of MeHg in experimental food chains formed by algae (70%) and zooplankton (13%) [59], but contrast in natural food chains with observed MeHg biomagnification [2, 31].

Impact of dietary MeHg on proteome in G. fossarum

Number and pattern of modulated proteins

We analyzed the whole proteome extracted from animals by shotgun proteomics and interpreted the high-resolution tandem mass spectra using a *G. fossarum* RNA-seq derived database. This proteogenomic approach led to 375,286 peptide-to-spectrum matches corresponding to 12,719 unique peptide sequences, resulting in 3,261 proteins identified with at least 2 peptides (Table S3). Globally, a total of 151 gammarid proteins were significantly modulated for the 4 treatment groups vs the control (Table S3). Among them, 78 were found more abundant, 67 were less abundant and 4 showed a higher abundance in intracellular but

were less abundant in cell wall treatments. Four distinct profiles of differentially abundant proteins were identified for each treatment (Figure 3). However, a higher overlap (6-8% of proteins) was observed in the same compartment, while only few proteins were shared between intracellular and cell wall fed gammarids (Figure 3A). Despite inter-individual variability is the main component of proteome variability in the organism analyzed in this study (Supplementary Figure 1) and as previously discussed [44], the differential analysis allowed the identification of rather distinct protein profiles for each treatment (Figure 3B).

The treatment affecting the higher number of proteins was the high MeHg intracellular treatment that modulated the abundance of 71 proteins, in line with the higher % of THg found in MSF. The low MeHg cell wall and intracellular compartments modulated 45 and 44 proteins respectively. The high MeHg cell wall treatment modulated 36 proteins, suggesting together with the higher proportion of THg in BDM, the occurrence of a higher detoxification.

Functional analysis of modulated proteins

The highest measured upregulation (Fold change 55x and 52x) and downregulation (-17x, -28x) were observed for proteins involved in 'cytoskeleton' for both cell wall treatments (Table 1). The Mass of these proteins are predicted between 42-35 kDa and could be involved in the visual increase of peaks in HMW on HPCL spectrograms (Figure S1), although because the area of HPLC eluting fractions is not strictly quantitative this comparison has to be made with caution. However, these proteins are known targets of both MeHg and IHg toxicity across taxa. For example, in copepods exposed to 50 $\mu g \cdot L^{-1}$ IHg in water, authors proposed that proteins assigned to this GO term (e.g. myosin) were involved in the cell reorganization to withstand Hg toxicity [60]. Proteins involved in cytoskeleton (actin, tubulin, keratin) that are essential for vesicle trafficking were significantly modified in fish and mammals exposed to IHg and MeHg supporting cytoskeleton disruption due to metal exposures [61, 62, 63, 64, 65]. In tuna muscle, binding of Hg to Beta-actin encompassed approximately 34% of Hg in the fish muscles[66]. Authors hypothesized that Hg binds to thiols in proteins. Here we observed that S represented 4.27 ± 0.08 % of residues in all samples (Table S4, Figure S3), not pointing to an increase of thiols in proteome of animals fed with Hg treatments.

Several modulated GO terms such as development/growth, energy metabolism, reproduction, locomotion/motility were common in all treatments (Table 2). To compare the impact of treatments on *G. fossarum* at a higher system level, we identified the most influent GOslim in the PCA as being autophagy (148), mitochondrion organization (18), ribosome biogenesis (164) and sulfur compound metabolic processes (1; Figure 4). Indeed, MeHg cell wall and

intracellular treatment decreased and increased the level of those GO terms respectively (Table 3), suggesting a different impact of the cell wall treatment than intracellular treatment on *G. fossarum* cell metabolism. GOslim identified for gammarids fed with MeHg from the intracellular compartment supported the induction of the cellular machinery likely for replacement of damaged proteins and warranting cell functions, while in animals fed with the cell wall compartment GOslim pointed mitochondrial perturbations and the induction of autophagy, ligase and nuclease activities supporting a perturbation of cell organization triggering repair pathways. In the same line, the contrasted modulation of GO terms related to gene expression (ribosome, RNA, DNA), protein maturation (ligase and transferase activities) and growth/development supports a higher modulation of proteome by intracellular MeHg, but a more detrimental impact to the cell metabolism of the cell wall MeHg. As such, the tolerance mechanisms triggered by the high-MeHg cell wall treatment resulting in a higher proportion of THg in BDM appeared to have a cost on fitness for those animals. Data are congruent with studies on one wild *G. fossarum* population exposed historically to Cd , evidencing the fitness costs and modification of toxicological sensitivities [67].

Here, differentially detected GO terms are in line with several known effects of MeHg. As mentioned above, the cytoskeleton participates in the transport of molecules and signaling by vesicular trafficking involved in autophagy [68, 69]. Autophagy is involved in elimination of aberrant or obsolete cellular structures. Mitochondria are known target of MeHg in animals [63, 70]. For example, in shrimps ^{203}Hg exposure by diet resulted in Hg bioaccumulation in organelles (10%) and HeSP (40%), while in *Crassostrea virginica* a 4 week-long exposure to 0.056 µM Hg through water resulted in 16x higher concentration in organelles than MTLPs [71,72]. Besides, MeHg was shown to depolarize mitochondrial membrane in synaptosomes [73]. Here, bioaccumulation in mitochondria was not investigated, but this GO term supported an interaction of Hg with this organelle in the high MeHg cell wall treatment. The GO term "gene regulation" was also abundant in copepods exposed to 50 $\mu g \cdot L^{-1}$ IHg in water and in Medaka exposed to 1 and 10 $\mu g \cdot L^{-1}$ IHg in water [60, 64].

On the other hand, some expected GO terms were not found as significantly different, notably proteins involved in reduction-oxidation (redox) metabolism and MTs in opposition with observation of a predominant BDM distribution for the high MeHg cell wall treatment. MeHg, IHg and other metals induce ROS production. Here, antioxidant enzymes that are often observed in response to IHg exposure, e.g. superoxide dismutases, peroxiredoxins and catalases [63, 64], were not significantly modulated at the protein level. Similarly, a proteomic

388 analysis of rats exposed to IHg by diet did not identify GO terms directly linked to redox,
389 despite the fact that they measured significantly increased lipid peroxidation by classical
390 biochemical analyses [63]. Nevertheless, here the GO term sulfur compound metabolic process
391 related to all chemical reactions and pathways involving sulfur-containing compounds (e.g.
392 methionine, cysteine, glutathione) strongly influenced the distribution in the PCA among
393 intracellular samples, while the proportion of Cysteine and Methionine residues in modulated
394 proteins didn't changed among treatments. This suggests the preexistence in the cytosol of a
395 sufficient pool of MTLP-MW proteins that could be involved in Hg-chelation in cytosol, as
396 also supported by the quite stable S proportion in residues of proteins for all treatments (Table
397 S4, Figure S3). Similarly, *G. fossarum* specimens collected *in situ* from a clean and a
398 contaminated river in Croatia showed increased soluble metal levels in gammarids in the
399 contaminated site, but similar MT concentrations in both sites [74]. In the same line,
400 *Caenorhabditis elegans* chronically exposed to 60 $mg \cdot L^{-1}$ MeHg showed no increase in mt
401 gene expression level after 15h exposure, while *mt*-gene loss-of-function mutants were
402 markedly more sensitive than wildtype to MeHg [75]. Nevertheless, previous studies in fish
403 showed that MTs correlated to Hg concentration in liver, but not muscles and gills [76]. Here the
404 proteomic analysis was conducted on whole organisms, potentially masking putative organ-
405 specific regulation. More investigation, outside the scope of the current study would be
406 necessary to conclude on the role of MTs in the tolerance to dietary MeHg in our
407 experimental conditions.
408 In conclusion, our analysis supported a sublethal stress likely coped by *G. fossarum* according
409 to the relative low number of modulated proteins in our experimental conditions. The analysis
410 revealed a correlation between protein abundance and Hg subcellular bioaccumulation in
411 MSF, but a different protein profile for each concentration, suggesting the occurrence of
412 several thresholds of regulation of the proteome. Data also suggested that in response to
413 increasing doses of MeHg, *G. fossarum* activated and/or deactivated some biochemical
414 processes to compensate the loss or impairment of other pathways caused by the toxicity of
415 MeHg. As such, defense mechanisms triggered by dietary MeHg appeared to have a cost for
416 the fitness of animals. Our experiment brought thus new insights on the specific effects of
417 MeHg in diet at sublethal concentration.
418 Our data in addition confirmed that Hg bound in cell walls of plants can be assimilated by *G.*
419 *fossarum*, which is consistent with its feeding strategy. The cell wall constituents are expected
420 to remain for a long period in the environment because of their recalcitrant nature. Here, data
421 point cell walls as a potential source of Hg transfers and toxicity to primary consumers.

Moreover, proteomic analysis revealed contrasted responses for intracellular and cell wall treatments, congruent with detoxification mechanisms and supporting that the different binding sites in shoots consequently caused different toxicity to consumers. In this context feeding behaviour of consumers appears instrumental for the fate and impact of Hg in food chains. In particular, the abundance of species and their feeding strategy need to be considered to adequately protect aquatic systems, as both will significantly influence the fate of Hg in local food webs. For example, the abundance of macrophytes in shallow water systems might favor the transfer of MeHg to food webs.

Aknowledgements

This research received financial support by Grand Reims in the frame of the Aquasurv chair. Authors thanks Dr Rebecca Beauvais-Flück and Mr Hervé Quéau for their help during exposures. The authors also benefitted from the French GDR "Aquatic Ecotoxicology" framework which aims at fostering stimulating scientific discussions and collaborations for more integrative approaches.

Supporting Information.

Table S1: Hg concentrations in water, *E. nuttallii* and *G. fossarum*; Table S2: Hg concentration in subcellular fractions; Table S3: list of identified proteins; Tables S4 to S6: proportion of thiols in proteins; Figure S1: HPLC chromatograms, Figure S2: Principal Component Analysis and Hierarchical clustering of samples, Figure S3: proportion of thiols in proteins against fold changes.

References

1. Boening, D. W., Ecological effects, transport, and fate of mercury: a general review. *Chemosphere* **2000,** *40*, 1335-1351

2. Bravo, A. G.; Cosio, C.; Amouroux, D.; Zopfi, J.; Chevalley, P.-A.; Spangenberg, J. E.; Ungureanu, V.-G.; Dominik, J., Extremely elevated methyl mercury levels in water, sediment and organisms in a Romanian reservoir affected by release of mercury from a chlor-alkali plant. *Wat Res* **2014,** *49*, 391-405

3. Lawrence, A. L.; Mason, R. P., Factors controlling the bioaccumulation of mercury and methylmercury by the estuarine amphipod *Leptocheirus plumulosus*. *Env Poll* **2001,** *111*, 217-31

4. UNEP, Global Mercury Assessment 2018: Sources, Emissions, Releases and Environmental Transport. Chemicals, Geneva, Switzerland. **2018**

5. Amos, H. M.; Jacob, D. J.; Streets, D. G.; Sunderland, E. M., Legacy impacts of all-time anthropogenic emissions on the global mercury cycle. *Glob Biogeoch Cyc* **2013,** *27*, 410-421

6. Obrist, D.; Kirk, J. L.; Zhang, L.; Sunderland, E. M.; Jiskra, M.; Selin, N. E., A review of global environmental mercury processes in response to human and natural perturbations: Changes of emissions, climate, and land use. *Ambio* **2018,** *47*, 116-140

7. Branfireun, B. A.; Cosio, C.; Poulain, A. J.; Riise, G.; Bravo, A. G., Mercury cycling in freshwater systems - An updated conceptual model. *Sci Tot Env* **2020,** *745*, 140906

8. Regier, N.; Larras, F.; Bravo, A. G.; Ungereanu, V. G.; Cosio, C., Hg bioaccumulation in the macrophyte *Elodea nuttallii* in the field and in microcosm: Hg in shoots accumulated from the water might involve Cu transporters. *Chemosphere* **2013,** *90*, 595-602

9. Regier, N.; Baerlocher, L.; Munsterkotter, M.; Farinelli, L.; Cosio, C., Analysis of the *Elodea nuttallii* transcriptome in response to mercury and cadmium pollution: development of sensitive tools for rapid ecotoxicological testing. *Env Sci Tech* **2013,** *47*, 8825-8834

10. Beauvais-Fluck, R.; Chaumot, A.; Gimbert, F.; Queau, H.; Geffard, O.; Slaveykova, V. I.; Cosio, C., Role of cellular compartmentalization in the trophic transfer of mercury species in a freshwater plant-crustacean food chain. *J Haz Mat* **2016,** *320*, 401-407

11. Beauvais-Fluck, R.; Gimbert, F.; Mehault, O.; Cosio, C., Trophic fate of inorganic and methyl-mercury in a macrophyte-chironomid food chain. *J Haz Mat* **2017,** *338*, 140-147

12. Lavoie, R. A.; Bouffard, A.; Maranger, R.; Amyot, M., Mercury transport and human exposure from global marine fisheries. *Sci Rep* **2018,** *8*, 6705

13. Wu, P.; Kainz, M. J.; Bravo, A. G.; Akerblom, S.; Sonesten, L.; Bishop, K., The importance of bioconcentration into the pelagic food web base for methylmercury biomagnification: A meta-analysis. *Sci Tot Env* **2019,** *646*, 357-367

14. Graves, S. D.; Kidd, K. A.; Batchelar, K. L.; Cowie, A. M.; O'Driscoll, N. J.; Martyniuk, C. J., Response of oxidative stress transcripts in the brain of wild yellow perch (*Perca flavescens*) exposed to an environmental gradient of methylmercury. *Comp Bioch Physiol Part C Tox Pharm* **2017,** *192*, 50-58

15. Lee, Y. H.; Kang, H. M.; Kim, D. H.; Wang, M.; Jeong, C. B.; Lee, J. S., Adverse effects of methylmercury (MeHg) on life parameters, antioxidant systems, and MAPK signaling pathways in the copepod *Tigriopus japonicus*. *Aq Tox* **2017,** *184*, 133-141

16. Gentes, S.; Maury-Brachet, R.; Feng, C.; Pedrero, Z.; Tessier, E.; Legeay, A.; Mesmer-Dudons, N.; Baudrimont, M.; Maurice, L.; Amouroux, D.; Gonzalez, P., Specific effects of dietary methylmercury and inorganic mercury in zebrafish (*Danio rerio*) determined by genetic, histological, and metallothionein responses. *Env Sci Tech* **2015,** *49*, 14560-14569

17. Wallace, W. G.; Lee, B.-G.; Luoma, S. N., Subcellular compartmentalization of Cd and Zn in two bivalves. I. Significance of metal-sensitive fractions (MSF) and biologically detoxified metal (BDM). In *Mar Ecol Prog Series*, 2003; *249*, 183-197.

18. Monteiro, F.; Lemos, L. S.; de Moura, J. F.; Rocha, R. C. C.; Moreira, I.; Di Beneditto, A. P.; Kehrig, H. A.; Bordon, I. C. A. C.; Siciliano, S.; Saint'Pierre, T. D.; Hauser-Davis, R. A., Subcellular metal distributions and metallothionein associations in rough-toothed dolphins (*Steno bredanensis*) from Southeastern Brazil. *MarPoll Bull* **2019,** *146*, 263-273

19. Gouveia, D.; Chaumot, A.; Charnot, A.; Almunia, C.; Francois, A.; Navarro, L.; Armengaud, J.; Salvador, A.; Geffard, O., Ecotoxico-proteomics for aquatic environmental monitoring: first *in situ* application of a new proteomics-based multibiomarker assay using caged amphipods. *Env Sci Tech* **2017,** *51*, 13417-13426

20. Mason, R. P.; Reinfelder, J. R.; Morel, F. M. M., Uptake, toxicity, and trophic transfer of mercury in a coastal diatom. *Env Sci Tech* **1996,** *30*, 1835-1845

21. Lee, C. S.; Fisher, N. S., Bioaccumulation of methylmercury in a marine copepod. *Env Tox Chem* **2017,** *36*, 1287-1293

22. Malviya, S.; Scalco, E.; Audic, S.; Vincent, F.; Veluchamy, A.; Poulain, J.; Wincker, P.; Iudicone, D.; de Vargas, C.; Bittner, L.; Zingone, A.; Bowler, C., Insights into global diatom distribution and diversity in the world's ocean. *Proc Nat Acad Sci* **2016,** *113*, E1516

23. Tadonleke, R. D.; Lazzarotto, J.; Anneville, O.; Druart, J.-C., Phytoplankton productivity increased in Lake Geneva despite phosphorus loading reduction. *J Plankton Res* **2009,** *31*, 1179-1194

24. Descy, J.-P.; Leitao, M.; Everbecq, E.; Smitz, J. S.; Deliege, J.-F., Phytoplankton of the River Loire, France: a biodiversity and modelling study. *J Plankton Res* **2012,** *34*, 120-135

25. Castro, R.; Pereira, S.; Lima, A.; Corticeiro, S.; Valega, M.; Pereira, E.; Duarte, A.; Figueira, E., Accumulation, distribution and cellular partitioning of mercury in several halophytes of a contaminated salt marsh. *Chemosphere* **2009,** *76*, 1348-1355

520 26. Larras, F.; Regier, N.; Planchon, S.; Poté, J.; Renaut, J.; Cosio, C., Physiological and
521 proteomic changes suggest an important role of cell walls in the high tolerance to metals of
522 *Elodea nuttallii*. *J Haz Mat* **2013,** *263*, 575-583
523 27. Valega, M.; Lima, A. I.; Figueira, E. M.; Pereira, E.; Pardal, M. A.; Duarte, A. C.,
524 Mercury intracellular partitioning and chelation in a salt marsh plant, *Halimione*
525 *portulacoides* (L.) Aellen: strategies underlying tolerance in environmental exposure.
526 *Chemosphere* **2009,** *74*, 530-6
527 28. Chaumot, A.; Geffard, O.; Armengaud, J.; Maltby, L.; Amiard-Triquet, C.; Amiard, J.-
528 C.; Mouneyrac, C., Chapter 11 - Gammarids as reference species for freshwater monitoring.
529 In *Aq Ecotox*, Academic Press: 2011; 253-280.
530 29. Boiche, A.; Lemoine, D. G.; Barrat-Segretain, M.-H.; Thiebaut, G., Resistance to
531 herbivory of two populations of *Elodea canadensis* Michaux and *Elodea nuttallii* Planchon
532 St. John. *Plant Ecol* **2011,** *212*, 1723-1731
533 30. Thiebaut, G.; Boiche, A.; Lemoine, D.; Barrat-Segretain, M.-H., Trade-offs between
534 growth and defence in two phylogenetically close invasive species. *Aq Ecol* **2017,** *51*, 405-
535 415
536 31. Cosio, C.; Fluck, R.; Regier, N.; Slaveykova, V. I., Effects of macrophytes on the fate
537 of mercury in aquatic systems. *Env Tox Chem* **2014,** *24*, 1225-1237
538 32. Hart, J. J.; Di Tomaso, J. M.; Linscott, D. L.; Kochian, L. V., Characterization of the
539 transport and cellular compartmentation of paraquat in roots of intact maize seedlings. *Pest*
540 *Bioch Physiol* **1992,** *43*, 212-222
541 33. Coulaud, R.; Geffard, O.; Xuereb, B.; Lacaze, E.; Queau, H.; Garric, J.; Charles, S.;
542 Chaumot, A., *In situ* feeding assay with *Gammarus fossarum* (Crustacea): Modelling the
543 influence of confounding factors to improve water quality biomonitoring. *Wat Res* **2011,** *45*,
544 6417-29
545 34. Besse, J. P.; Coquery, M.; Lopes, C.; Chaumot, A.; Budzinski, H.; Labadie, P.;
546 Geffard, O., Caged *Gammarus fossarum* (Crustacea) as a robust tool for the characterization
547 of bioavailable contamination levels in continental waters: towards the determination of
548 threshold values. *Wat Res* **2013,** *47*, 650-60
549 35. Qualité de l'eau - Mesures moléculaires, physiologiques et comportementales chez le
550 gammare (crustacé amphipode) - Partie 3 : mesure du taux d'alimentation.
551 https://norminfo.afnor.org/consultation/xp-t90-722-3/qualite-de-leau-mesures-moleculaires-
552 physiologiques-et-comportementales-chez-le-gammare-crustace-amphipode-partie-3/93355

553 36. Geffard, A.; Sartelet, H.; Garric, J.; Biagianti-Risbourg, S.; Delahaut, L.; Geffard, O.,
554 Subcellular compartmentalization of cadmium, nickel, and lead in *Gammarus fossarum*:
555 Comparison of methods. *Chemosphere* **2010,** *78*, 822-829
556 37. Gimbert, F.; Geffard, A.; Guedron, S.; Dominik, J.; Ferrari, B. J. D., Mercury tissue
557 residue approach in *Chironomus riparius*: Involvement of toxicokinetics and comparison of
558 subcellular fractionation methods. *Aq Tox* **2016,** *171*, 1-8
559 38. Rosabal, M.; Hare, L.; Campbell, P. G. C., Assessment of a subcellular metal
560 partitioning protocol for aquatic invertebrates: preservation, homogenization, and subcellular
561 fractionation. *Limnol Ocean Met* **2014,** *12*, 507-518
562 39. Cardon, P.-Y.; Caron, A.; Rosabal, M.; Fortin, C.; Amyot, M., Enzymatic validation of
563 species-specific protocols for metal subcellular fractionation in freshwater animals. *Limnol*
564 *Ocean Met* **2018,** *16*, 537-555
565 40. USEPA, Method 1631: Mercury in water by oxidation, purge and trap, and CVAFS.
566 *Office of Water, Revision E* **2002**,
567 41. USEPA, Method 1630: Methyl mercury in water by distillation, aqueous ethlylation,
568 purge and trap, and CVAFS. *Office of Water, draft* **2001**,
569 42. Hammerschmidt, C. R.; Fitzgerald, W. F., Methylmercury in mosquitoes related to
570 atmospheric mercury deposition and contamination. *Env Sci Technol* **2005,** *39*, 3034-9
571 43. R Development Core Team, R: a language and environment for statistical computing.
572 R Foundation for Statistical Computing. **2013**, 12
573 44. Cogne, Y.; Almunia, C.; Gouveia, D.; Pible, O.; François, A.; Degli-Esposti, D.;
574 Geffard, O.; Armengaud, J.; Chaumot, A., Comparative proteomics in the wild: Accounting
575 for intrapopulation variability improves describing proteome response in a *Gammarus pulex*
576 field population exposed to cadmium. *Aq Tox* **2019,** *214*, 105244
577 45. Hartmann, E. M.; Allain, F.; Gaillard, J. C.; Pible, O.; Armengaud, J., Taking the
578 shortcut for high-throughput shotgun proteomic analysis of bacteria. *Meth Mol Biol* **2014,**
579 *2014*, 275-85
580 46. Gouveia, D.; Cogne, Y.; Gaillard, J.-C.; Almunia, C.; Pible, O.; François, A.; Degli-
581 Esposti, D.; Geffard, O.; Chaumot, A.; Armengaud, J., Shotgun proteomics datasets acquired
582 on *Gammarus pulex* animals sampled from the wild. *Dat Brief* **2019,** *27*, 104650
583 47. Gouveia, D.; Grenga, L.; Pible, O.; Armengaud, J., Quick microbial molecular
584 phenotyping by differential shotgun proteomics. *Env Microbiol* **2020**, 22: 2996-3004

48. Trapp, J.; Geffard, O.; Imbert, G.; Gaillard, J.-C.; Davin, A.-H.; Chaumot, A.; Armengaud, J., Proteogenomics of *Gammarus fossarum* to document the reproductive system of amphipods. *Mol Cell Prot* **2014,** *13*, 3612

49. Gallais, F.; Pible, O.; Gaillard, J. C.; Debroas, S.; Batina, H.; Ruat, S.; Sandron, F.; Delafoy, D.; Gerber, Z.; Olaso, R.; Gas, F.; Bellanger, L.; Deleuze, J. F.; Grenga, L.; Armengaud, J., Heterogeneity of SARS-CoV-2 virus produced in cell culture revealed by shotgun proteomics and supported by genome sequencing. *Anal Bioanal Chem* **2021,** *20*, 1-11

50. Perez-Riverol, Y.; Csordas, A.; Bai, J.; Bernal-Llinares, M.; Hewapathirana, S.; Kundu, D. J.; Inuganti, A.; Griss, J.; Mayer, G.; Eisenacher, M.; Perez, E.; Uszkoreit, J.; Pfeuffer, J.; Sachsenberg, T.; Yilmaz, S.; Tiwary, S.; Cox, J.; Audain, E.; Walzer, M.; Jarnuczak, A. F.; Ternent, T.; Brazma, A.; Vizcaino, J. A., The PRIDE database and related tools and resources in 2019: Improving support for quantification data. *Nucl Ac Res* **2019,** *47*, D442-D450

51. Buchfink, B.; Xie, C.; Huson, D. H., Fast and sensitive protein alignment using DIAMOND. *Nat Meth* **2014,** *12*, 59-60

52. Trapp, J.; Gouveia, D.; Almunia, C.; Pible, O.; Degli Esposti, D.; Gaillard, J.-C.; Chaumot, A.; Geffard, O.; Armengaud, J., Digging deeper into the pyriproxyfen-response of the amphipod *Gammarus fossarum* with a next-generation ultra-high-field orbitrap analyser: new perspectives for environmental toxicoproteomics. *Front Env Sci* **2018,** *6*, 54

53. Carvalho, P. C.; Lima, D. B.; Leprevost, F. V.; Santos, M. D. M.; Fischer, J. S. G.; Aquino, P. F.; Moresco, J. J.; Yates, J. R.; Barbosa, V. C., Integrated analysis of shotgun proteomic data with PatternLab for proteomics 4.0. *Nat Protocols* **2016,** *11*, 102-117

54. Znidaric, M. T.; Falnoga, I.; Skreblin, M.; Turk, V., Induction of metallothionein-like proteins by mercury and distribution of mercury and selenium in the cells of hepatopancreas and gill tissues in mussel *Mytilus galloprovincialis*. *Biol Trace El Res* **2006,** *111*, 121-135

55. Dang, F.; Wang, W. X., Subcellular controls of mercury trophic transfer to a marine fish. *Aq Tox* **2010,** *99*, 500-506

56. Park, J.; Song, W. Y.; Ko, D.; Eom, Y.; Hansen, T. H.; Schiller, M.; Lee, T. G.; Martinoia, E.; Lee, Y., The phytochelatin transporters AtABCC1 and AtABCC2 mediate tolerance to cadmium and mercury. *Plant J* **2012,** *69*, 278-288

57. Gupta, M.; Tripathi, R. D.; Rai, U. N.; Chandra, P., Role of glutathione and phytochelatin in *Hydrilla verticillata (lf) Royle* and *Vallisneria spiralis* L. under mercury stress. *Chemosphere* **1998,** *37*, 785-800

58. Tai, H. C.; Lim, C., Computational studies of the coordination stereochemistry, bonding, and metal selectivity of mercury. *J Phys Chem A* **2006,** *110*, 452-462

59. Pickhardt, P. C.; Folt, C. L.; Chen, C. Y.; Klaue, B.; Blum, J. D., Impacts of zooplankton composition and algal enrichment on the accumulation of mercury in an experimental freshwater food web. *Sci Tot Env* **2005,** *339*, 89-101

60. Xu, X.; Shi, L.; Wang, M., Comparative quantitative proteomics unveils putative mechanisms involved into mercury toxicity and tolerance in *Tigriopus japonicus* under multigenerational exposure scenario. *Env Poll* **2016,** *218*, 1287-1297

61. Keyvanshokooh, S.; Vaziri, B.; Gharaei, A.; Mahboudi, F.; Esmaili-Sari, A.; Shahriari-Moghadam, M., Proteome modifications of juvenile beluga (*Huso huso*) brain as an effect of dietary methylmercury. *Comp Biochem Physiol Part D Genom Prot* **2009,** *4*, 243-248

62. Berg, K.; Puntervoll, P.; Valdersnes, S.; Goksoyr, A., Responses in the brain proteome of Atlantic cod (*Gadus morhua*) exposed to methylmercury. *Aq Tox* **2010,** *100*, 51-65

63. Correa, M. G.; Bittencourt, L. O.; Nascimento, P. C.; Ferreira, R. O.; Aragao, W. A. B.; Silva, M. C. F.; Gomes-Leal, W.; Fernandes, M. S.; Dionizio, A.; Buzalaf, M. R.; Crespo-Lopez, M. E.; Lima, R. R., Spinal cord neurodegeneration after inorganic mercury long-term exposure in adult rats: Ultrastructural, proteomic and biochemical damages associated with reduced neuronal density. *Ecotox Env Saf* **2020,** *191*, 110159

64. Wang, M.; Wang, Y.; Zhang, L.; Wang, J.; Hong, H.; Wang, D., Quantitative proteomic analysis reveals the mode-of-action for chronic mercury hepatotoxicity to marine medaka (*Oryzias melastigma*). *Aq Tox* **2013,** *130-131*, 123-131

65. Quintá, H. R.; Galigniana, N. M.; Erlejman, A. G.; Lagadari, M.; Piwien-Pilipuk, G.; Galigniana, M. D., Management of cytoskeleton architecture by molecular chaperones and immunophilins. *Cell Sign* **2011,** *23*, 1907-1920

66. Nong, Q.; Dong, H.; Liu, Y.; Liu, L.; He, B.; Huang, Y.; Jiang, J.; Luan, T.; Chen, B.; Hu, L., Characterization of the mercury-binding proteins in tuna and salmon sashimi: Implications for health risk of mercury in food. *Chemosphere* **2021,** *263*, 128110.

67. Vigneron, A.; Geffard, O.; Coquery, M.; Francois, A.; Queau, H.; Chaumot, A., Evolution of cadmium tolerance and associated costs in a *Gammarus fossarum* population inhabiting a low-level contaminated stream. *Ecotox* **2015,** *24*, 1239-1249

68. Amaya, C.; Fader, C. M.; Colombo, M. I., Autophagy and proteins involved in vesicular trafficking. *FEBS Letters* **2015,** *589*, 3343-3353

69. Kast, D. J.; Dominguez, R., The cytoskeleton-autophagy connection. *Cur biol CB* **2017,** *27*, R318-R326

70. Ferreira, F. F.; Nazari, E. M.; Muller, Y. M. R., MeHg causes ultrastructural changes in mitochondria and autophagy in the spinal cord cells of chicken embryo. *J Toxicol* **2018,** *2018*, 8460490

71. Seebaugh, D. R.; Wallace, W. G., Assimilation and subcellular partitioning of elements by grass shrimp collected along an impact gradient. *Aq Tox* **2009,** *93*, 107-115

72. Mass Fitzgerald, A.; Zarnoch, C. B.; Wallace, W. G., Examining the relationship between metal exposure (Cd and Hg), subcellular accumulation, and physiology of juvenile *Crassostrea virginica*. *Env Sci Poll Res* **2019,** *26*, 25958-25968

73. Hare, M. F.; Atchison, W. D., Comparative action of methylmercury and divalent inorganic mercury on nerve terminal and intraterminal mitochondrial membrane potentials. *J Pharmacol Exp Ther* **1992,** *261*, 166-72

74. Filipovic Marijic, V.; Dragun, Z.; Sertic Peric, M.; Matonickin Kepcija, R.; Gulin, V.; Velki, M.; Ecimovic, S.; Hackenberger, B. K.; Erk, M., Investigation of the soluble metals in tissue as biological response pattern to environmental pollutants (*Gammarus fossarum* example). *Chemosphere* **2016,** *154*, 300-309

75. Helmcke, K. J.; Aschner, M., Hormetic effect of methylmercury on *Caenorhabditis elegans*. *Tox Appl Pharmacol* **2010,** *248*, 156-164

76. Bebianno, M. J.; Santos, C.; Canario; J.; Gouveia, N.; Sena-Carvalho, D.; Vale, C., Hg and metallothionein-like proteins in the black scabbardfish *Aphanopus carbo*. *Food Chem Tox* **2007,** *45*, 1443-1452

Table 1. List of the five most up and down-detected proteins in each treatment. Abundance vs control (Log2 fold change), annotation, % identities and e-value are listed. Values in bold are significantly different to control (p-value <0.05 calculated with univariate statistic: Ttest).

Functional annotation	% sequence identity	Expect value	I-low	I-high	C-low	C-high
Cell structure						
actin, cytoplasmic 1	51.3	1.5e-58	1.1	-1.8	**55.2**	**53.0**
myosin light chain alkali-like	53.8	5.9e-23	-2.3	**-5.3**	2.2	1.7
tubulin alpha-3 chain	75.2	7.1e-135	5.1	**18.1**	-1.7	-1.7
myosin heavy chain, muscle-like isoform X18	76.1	1.7e-70	1.1	6.1	**-11.5**	**-4.9**
myosin heavy chain type b	58.7	2.6e-69	-1.0	5.9	**-7.1**	**-7.0**
collagen alpha-1, IV, chain precursor, putative	63.5	1.2e-61	-1.7	-2.7	-2.3	**-7.9**
myosin heavy chain, partial	83.8	2.9e-79	2.2	17.1	**-17.3**	**-28.3**
Energy metabolism						
ADP/ATP translocase 3-like	94	1.4e-44	**-8.0**	-2.2	7.2	5.7
fructose-bisphosphate aldolase	85.7	5.8e-31	**7.0**	**2.7**	1.1	-1.0
sucrase-isomaltase, intestinal	59.8	9,00E-102	**-6.4**	-2.6	-2.1	-1.1
glycogen phosphorylase	67.4	2.5e-98	**6.4**	**8.6**	-1.9	-1.2
aconitate hydratase, mitochondrial	91.6	2.4e-168	3.9	**6.5**	1.4	-1.2
endoglucanase E-4	72	5.1e-147	**-4.4**	**-5.4**	-3.0	-1.2
malate dehydrogenase, cytoplasmic	87.8	4.1e-161	**3.9**	**6.0**	-1.1	-1.6
enolase isoform X1	77.7	1.7e-113	**-14.1**	-3.0	-6.0	-5.1
family 7 cellobiohydrolase	77.9	6.7e-61	1.4	-8.9	-2.1	**-7.9**
Response to stress						
endoplasmin-like isoform X1	78.5	5.2e-177	**3.4**	2.2	**6.8**	**7.1**
oplophorus-luciferin 2-monooxygenase non-catalytic subunit	34	4.4e-46	2.1	1.7	**5.3**	3.3
glucosylceramidase-like	73.6	4.5e-56	**-4.1**	**-6.2**	2.1	2.1
phosphate carrier protein, mitochondrial-like	81.3	2.5e-119	-2.0	**-7.5**	1.2	1.5
hemolymph clottable protein-like isoform X1	31.6	1.1e-06	**4.3**	3.1	2.8	1. 3
putative glucosylceramidase 3	63.8	7.9e-42	-1.3	-1.2	**4.5**	1.0

dehydrogenase/reductase SDR family member 4	56.1	3.5e-45	**4.4**	-1.3	1.8	-1.0
beta-1,3-glucan binding protein	38	3.7e-41	-1.5	3.1	**-6.5**	**-8.6**
endoplasmin-like isoform X2	70	5.5e-135	-1.0	2.4	**-8.8**	**-8.7**
Others						
putative glucosylceramidase 3	55.8	6.2e-115	1.1	-2.5	2.5	**6.2**
putative ferric-chelate reductase 1 homolog	30.3	1.7	1.3	-3.1	4.3	**5.2**
uncharacterized protein	49.5	9.2e-43	1.1	4.0	2.3	**15.3**
uncharacterized protein	29.9	7.9e-55	1.1	-1.2	**4.5**	2.9
uncharacterized protein	56	4.2e-61	**6.7**	**7.5**	3.2	1.7
uncharacterized protein	61.9	1.4e-78	-1.9	**-4.7**	-1.7	1.1

Table 2. Ratio of GOslim terms for molecular function (MF), biological process (BP) and cellular compartment (CC) showing opposite trends for *G. fossarum* feeding on the low or high MeHg contaminated intracellular (I) or cell wall (C) compartment vs respective controls *of E. nuttallii*. Values in bold are significantly different to control (Log2 fold change, *p-value <0.05 calculated with univariate statistic: Ttest).

		I-low	**I-high**	**C-low**	**C-high**
GOslim_MF	cytoskeletal protein binding	**3.7***	**1.7***	-3.0	-1.1
GOslim_MF	enzyme binding	**2.0***	1.7	-1.8	-2.0
GOslim_MF	DNA binding	**3.0***	1.9	**-2.2***	**-1.1***
GOslim_MF	ATPase activity	**3.0***	1.3	-2.0	-1.2
GOslim_BP	plasma membrane organization	**3.0***	**1.7***	**2.5***	-2.8
GOslim_BP	anatomical structure development	**1.1***	1.1	-2.0	**-1.1***
GOslim_BP	anatomical structure formation involved in morphogenesis	**3.7***	**1.6***	-1.4	**-1.4***
GOslim_BP	circulatory system process	**2.9***	1.5	-3.6	-2.3
GOslim_BP	embryo development	**3.6***	1.5	-3.2	**-1.8***
GOslim_BP	reproduction	**1.7***	1.5	-1.9	**-1.5***
GOslim_BP	growth	**1.1***	**2.0***	-2.8	-2.4
GOslim_BP	locomotion	**1.7***	1.4	-1.3	**-1.4***
GOslim_BP	cell motility	**3.8***	1.4	-2.2	**-1.5***
GOslim_CC	chromosome	**4.2***	1.1	-3.7	-1.2
GOslim_CC	cytosol	**1.0***	**1.3***	-1.5	-1.3
GOslim_CC	nucleoplasm	**1.4***	1.8	**-1.3***	**-2.3***
GOslim_CC	microtubule organizing center	**5.5***	6.0	2.9	-2.8
GOslim_CC	protein-containing complex	**1.1***	1.3	-1.2	**-1.1***

Table 3. Ratio of GO terms responding to concentration for *G. fossarum* feeding on the low and high MeHg contaminated intracellular (I) and cell wall compartment (C) vs respective controls *of E. nuttallii* (Log2 fold change; *p-value <0.05; #N/A GO term not found for the treatment).

		GO Term # on PCA	I-low	I-high	C-low	C-high
GOslim_BP	autophagy	148	-5.1*	0.8	-0.2	4.8
GOslim_BP	mitochondrion organization	18	-2.9*	0.6	-4.4	4.8
GOslim_BP	ribosome biogenesis	164	#N/A	2.4	-5.6	#N/A
GOslim_CC	microtubule organizing center	198	5.5*	6.0	2.9	-2.8
GOslim_CC	ribosome	207	#N/A	2.4	-5.6	-4.9*
GOslim_MF	transferase activity, transferring glycosyl groups	5	5.9*	5.8*	-5.1	#N/A
GOslim_MF	ligase activity	99	0.3	0.7	-4.4	4.8
GOslim_MF	rRNA binding	101	#N/A	2.1	-4.8	-4.9*
GOslim_MF	structural constituent of ribosome	75	#N/A	2.4	-5.6	-4.9*

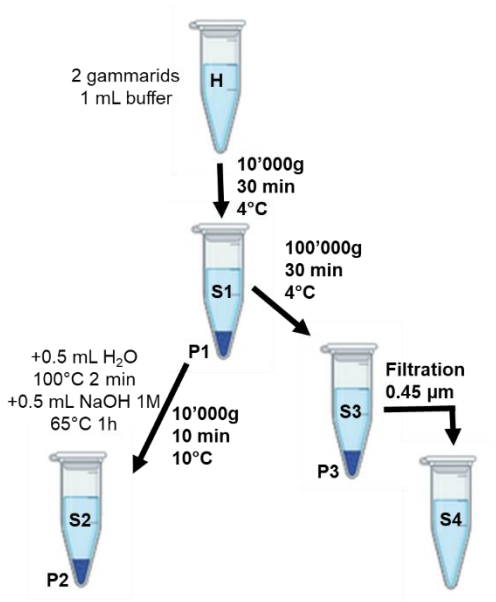

Figure 1. main steps of differential centrifugation protocol.

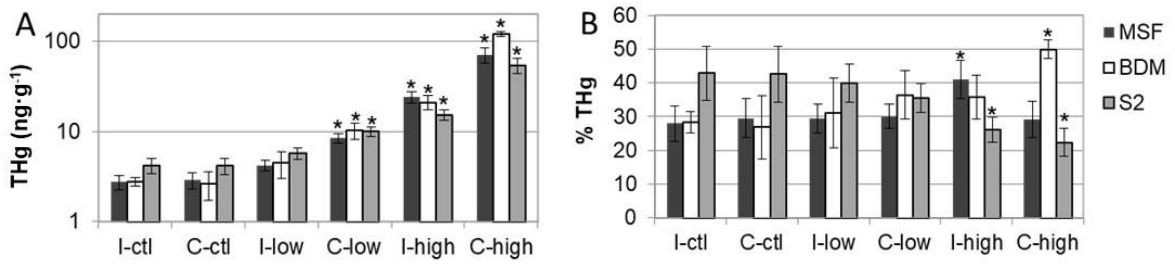

Figure 2. Concentration ($ng \cdot g^{-1}$; mean ± sd; A) and proportion (%; B) of THg measured in MSF, BDM and debris (S2) for *G. fossarum* feeding on the MeHg contaminated intracellular (I) or cell wall (C) compartment *of E. nuttallii* (*$p<0.05$ vs control; n = 3).

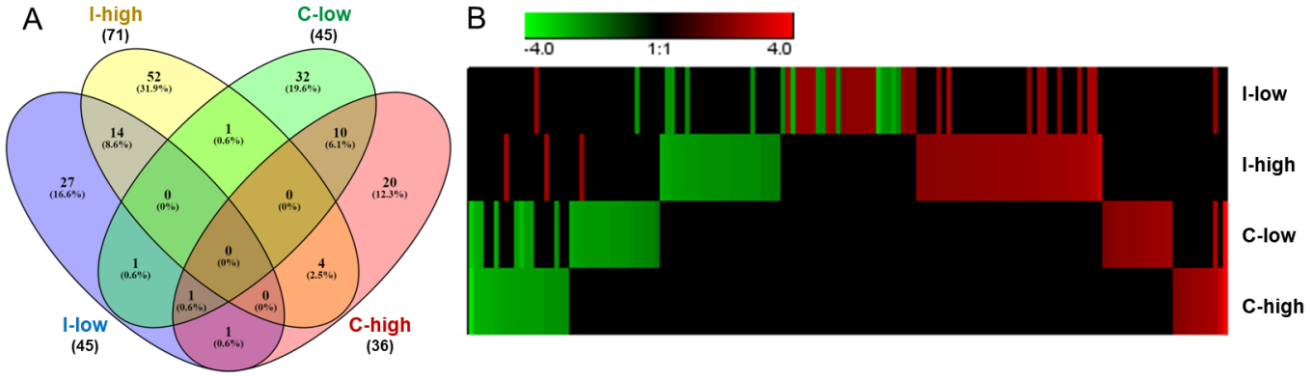

Figure 3: Venn diagram (A) and heatmap (Log2 fold change) (B) of differentially abundant proteins in *G. fossarum* feeding 7 days on the low or high MeHg contaminated intracellular (I) or cell wall (C) vs control (p-value <0.05). Maximum of heatmap is set to 4 for visibility of smaller fold changes (see Table 1 for identification of most modulated proteins).

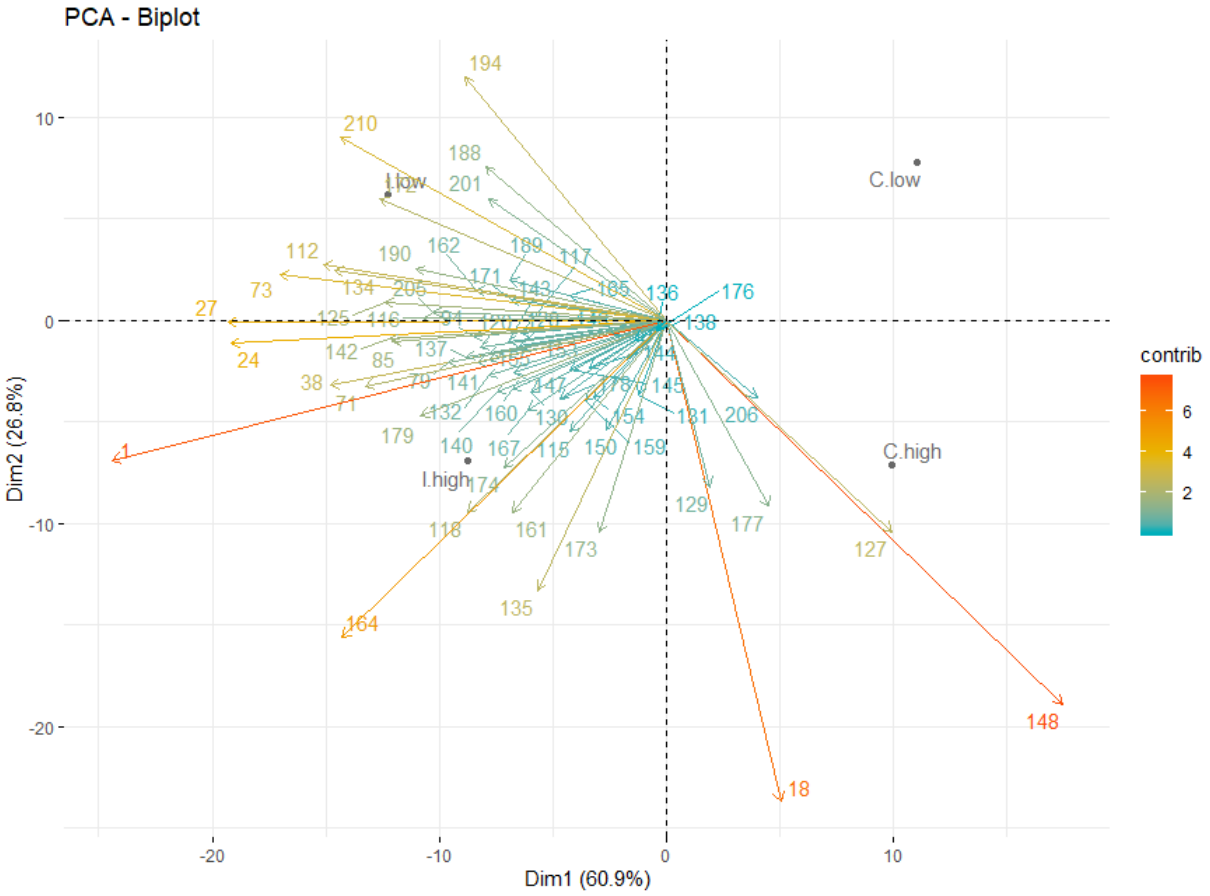

Figure 4. PCA of GOslim terms according to biological processes in *G. fossarum* feeding 7 days on the low or high MeHg contaminated intracellular (I) or cell wall (C) vs control.